COMMUNICATION

Check for updates

Chirality enhancement in macro-chiral liquid crystal nanoparticles†

Huanan Yu, [a] Chris Welch, [a] Wentao Qu, [b] Christopher J. Schubert, [a] Feng Liu, [b] Giuliano Siligardi [c] and Georg H. Mehl ⋆[ab]

The amplification of molecular chirality by metal nanoparticles (NPs) is an important and rapidly evolving field in nanomaterial research with wide applications in smart materials, catalysis, and solvent–solute interactions. Here we present the results of the synthesis of gold nanoparticles (AuNPs) functionalized both with chiral ligands based on the binaphthol motif and with nematogenic groups (ChirAuLC). The materials were characterized chemically and the ratios between chiral groups and LC groups was determined. Synchrotron radiation circular dichroism (SRCD) and synchrotron based X-ray diffraction (XRD) studies show that the AuNPs favoured by the LC state arrange themselves into ordered columns and a helical superstructure appears in the mesophase of collective NPs. A specific focus has been the investigation of the chiral induction of ChirAuLC composites in two different nematic LC hosts. For a number of selected mixtures, the helical twisting power (HTP) of these NPs in systems was calculated from systematic optical observations based on optical polarizing microscopy (OPM). The experimental data show that the HTP of the investigated ChirAuLC composite is significantly larger than that of free "small molecule" chiral groups when dispersed in the same LC host and the chiral transfer efficiency of ChirAuLC is higher than NPs functionalized only with chiral groups (ChirAuNP). This is new and can be explained by a combination of a surface chirality and the domino effect of bound mesogens interacting with the bulk.

The understanding and utilisation of information transfer is one of the most important questions in sciences associated with matter.[1,2] Examples are the transfer of genetic information with DNA or RNA where specific forms are crucial in cellular information processes.[3,4] For proteins, chirality of the amino acids is critical for the folding and function of these biological

New concepts

The measurement and understanding of chirality transfer to a chemically non-chiral bulk is one of the most important and fascinating challenges impacting on all areas of materials science. The addition of a small amount dopant can change the macroscopic properties of a suitable system completely. A spectacular effect is in liquid crystals, where photonic properties, such as the selective reflection wavelength can be addressed with great precision. Small nanometric sized gold nanoparticles functionalized with chiral groups dispersed in liquid crystals are often more efficient for chirality transfer than comparable amounts of small chiral molecules and this can be attributed to a type of dispersed surface effect of these systems. A modular approach to this challenge shows that using nanoparticles functionalized chemically with both chiral groups and liquid crystal groups enhances the interaction of these system with LC matrices. A significant and systematic enhanced chirality transfer from the nanoparticles to the bulk can be quantified. This can be rationalized as a combination of a distributed chiral surface and "sergeant-soldier" effects where bound LC groups enhance the chirality transmission; in other words the modular constructed NP systems act as well dispersed macrochiral species. Crucially in our view, this concept is very versatile and easily adaptable.

polymers.[5–7] Specific folding states are of a lower energy state and are thus favoured.[8] The chiral bias of the subunits is a precondition for the intended mode of operation. For the use of designed materials and the operation of related technology, such a bias is crucial; examples are information display devices,[9–13] where the response at a design input voltage is at a lower energy than other response pathways.[14] Common is that chirality is employed effectively and efficiently.

Typically, incorporation of such molecules into linear polymers reduces their miscibility in the liquid crystal matrix.[15,16] Very few chemical subunits are actually chiral; their chirality is amplified by impacting on the organisation of their surroundings: for biological systems, this is an outcome of selection pressure while for designed systems,[17,18] the understanding is ongoing and still needs to be advanced. For linear polymers, the so called "Sergeant-Soldier"[19–21] and the related "domino" approach has been pioneered. In low dimensional liquid crystal (LC) phases such as the nematic phase, the addition of small chiral molecules

[a] Department of Chemistry, University of Hull, Hull, HU6 7RX, UK.
E-mail: g.h.mehl@hull.ac.uk
[b] State Key Laboratory for Mechanical Behaviour of Materials, Shaanxi International Research Centre for Soft Matter, Xi'an Jiaotong University, Xi'an, P. R. China
[c] Diamond Light Source, Harwell, Didcot, OX11 0DE, UK

perturbs the packing and a chiral phase ensues.[22–25] Considerable effort has been made linking chiral groups or chiral LC groups to nanometric sized particles (NPs).[26] For such systems chirality transfer has been explained by either favourable interactions with the LC groups or chiral plasmonic interactions have been proposed.[27]

Here we show that for NP systems, functionalized with both LC and chiral groups, a synergistic amplification of chirality is obtained. Conceptually, our novel approach is based on the inherent advantageous properties of intrinsically liquid crystal chiral NPs in LC matrices. Based on this concept we can show that the combination of a chiral surface concept of functionalized NPs with that of a modified "sergeant-soldier" approach, results in significantly enhanced chirality transfer.

We prepared sets of NPs in the size range centering around 1.9 nm and 4.5 nm, we capped them with hexylthiol groups to stabilize them and prepared samples in exchange reactions where either a chiral binaphthol group (**L2**, see Chart 1) or **L2** and a liquid crystal mesogen (**L1**) was introduced. The NPs were characterized by transmission electron microscopy (TEM), UV-Vis spectroscopy, thermogravimetric analysis (TGA), elemental analysis (EA) and ^{1}H-NMR spectroscopy to identify the size and composition of the nanocomposites.[28,29] The self-assembly properties were identified with synchrotron-based X-ray diffraction (XRD), optical polarizing microscopy (OPM) and differential scanning calorimetry (DSC). Chirality was measured in thin films using synchrotron radiation circular dichroism (SRCD) spectroscopy. For discrete compositions with two LC hosts, detailed helical pitch measurements were performed by using the Cano wedge cell method and optical cells promoting homeotropic alignment. This allowed us to calculate the helical twisting

power (HTP), a measure for the ability of a chiral dopant to twist a nematic LC host.[30–32] The chiroptical properties of these NPs will be discussed and compared to structurally related materials.

The synthesis of the nematogen (**L1**) and the 1-hexanethiol-functionalized AuNPs was accomplished following a route described earlier.[33] An exchange reaction introduced binaphthol (S) based chiral groups (**L2**) and the nematogen (**L1**) was attached to hexylthiol capped AuNPs via thioalkyl chains (see Scheme S1, ESI†). Following purification by washing with ethanol, AuNPs coated with both **L2** and nematogen **L1** were obtained, denoted as **ChirAuLC**. Similarly, AuNPs coated with only chiral groups were prepared as a comparison, termed as **ChirAuNP**.

As the main host for the subsequent research, the LC properties of **L1** were characterized by OPM and DSC (see Fig. S1, ESI†) verifying the exclusive nematic behaviour between the melting point (M.P.) at 47.2 °C and the isotropisation at 63.8 °C. Hence **L1** was judged to be an ideal ligand as well as test matrix to measure the effects of chirality.

The purified NPs were first characterized by (TEM) and UV-Vis spectroscopy (see Fig. 1 and Fig. S3, S4, ESI†). As no obvious surface plasmon resonance (SPR) peaks were measured in the visible, this indicates that these NPs are smaller than 5 nm in diameter, confirmed too by TEM micrographs in Fig. 1a and b.[34] Compared with the AuNPs in Fig. 1a, **ChirAuLC1** in Fig. 1b shows a higher level of organisation on the surface of the TEM grid (copper). However unambiguous identification of specific super-structures is tenuous, due to the small sizes of the NPs and the resulting large effects of small variations in the size distribution. To address this problem, larger NPs were prepared. For **AuNP2** and **ChirAuLC2** (see Fig. S4c, ESI†), a SPR band is observed with an absorption maximum (λ_{max}) at λ_{max} = 528 nm, confirming the size close to 5 nm in diameter, evident too from TEM images shown in Fig. 1d and e.

Overall the sizes of the two pairs of NPs as obtained from TEM data **AuNP1**, **ChirAuLC1** and **AuNP2**, **ChirAuLC2** are 1.9, 2.2, and 4.5, 5.1 nm, respectively. The shift to larger sizes in both pairs of the further functionalized NPs is often observed and is attributed to the loss of smaller particles in additional purification steps.[35] The purity and functionalization of NPs, specifically the absence of unreacted ligands was confirmed by ^{1}H-NMR spectroscopy (see Fig. S7, ESI†). A typical feature is broadened ^{1}H peaks caused by the reduced mobility of alkyl chains when attached onto NPs. The lack of distinct high resolution signals confirms the absence of free ligands.

For the tightly packed **ChirAuLC2** (Fig. 1e) NPs on the TEM grid a distinct ordered organisation (see inset) suggesting self-organisation is detectable. Powder small-angle X-ray scattering (SAXS) of larger NPs (see Fig. S5 and S6, ESI†) show a columnar phase with a $p2$ lattice symmetry for both **ChirAuNP2** and **ChirAuLC2**. The peak positions of the columnar phase for **ChirAuNP2** with the lattice parameters: a = 7.42 nm, b = 6.30 nm, γ = 77.1° and for **ChirAuLC2** of: a = 6.98 nm, b = 5.93 nm, γ = 76.9° respectively are given in Tables S2 and S3 (ESI†), respectively. The reduction in the lattice parameters a and b for **ChirAuLC2** compared to **ChiralAuNP2** can be rationalized by the ordering of the aromatic ligands attached to the NPs in the LC state. The organic corona is
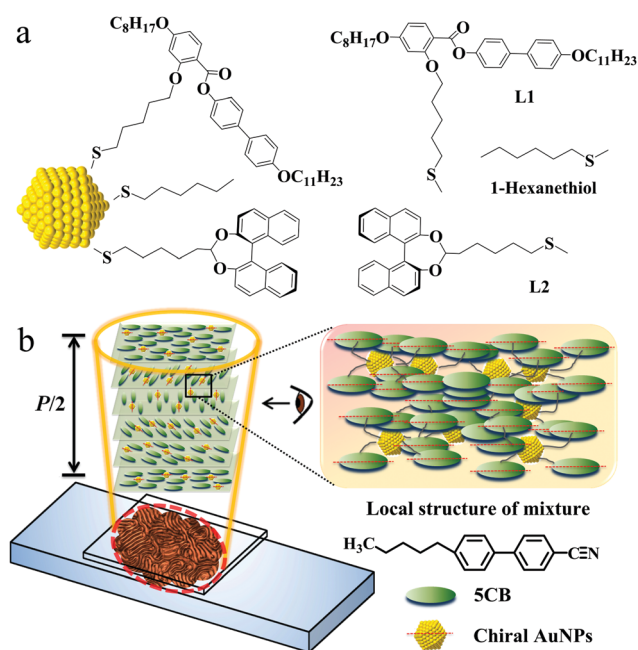

Chart 1 (a) Sketch of a segment of functionalized gold nanoparticle **ChirAuLC**, (b) cartoon introducing the concept of induced chiral structure in host 5CB by the macro-chiral liquid crystal nanoparticles (**ChirAuLC**).
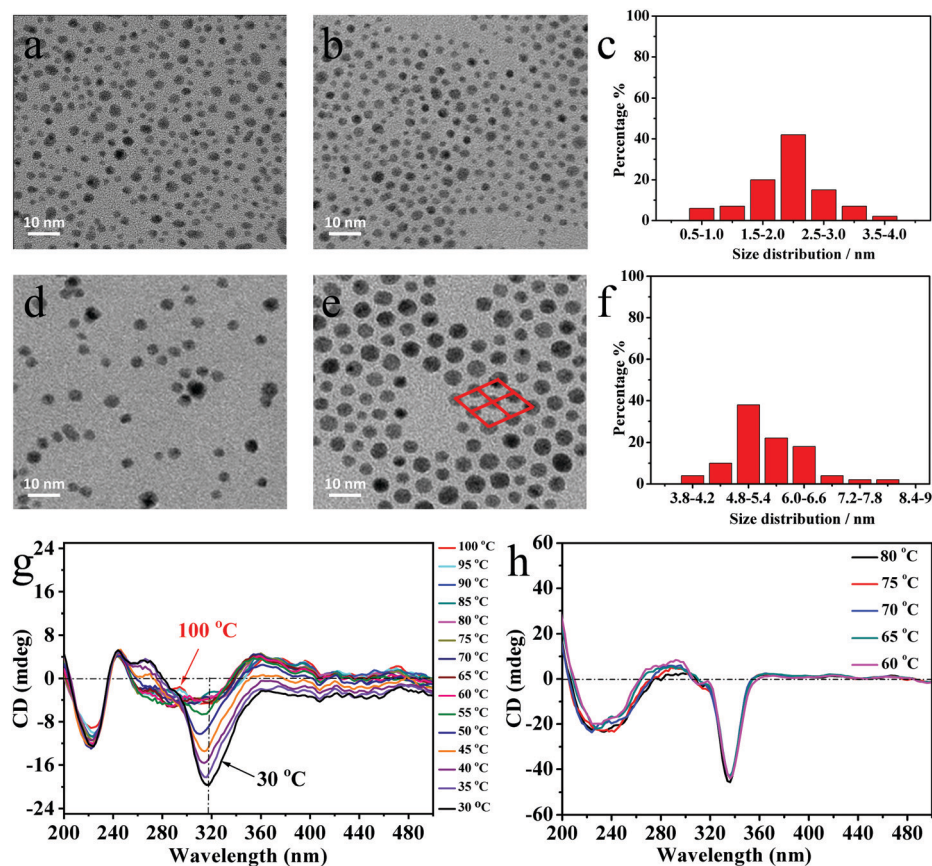
Fig. 1   TEM pictures of (a) thiol-capped **AuNP1**, (b) **ChirAuLC1**, (c) size distribution graph of **ChirAuLC1**, (d) thiol-capped **AuNP2**, (e) **ChirAuLC2**, (f) size distribution graph of **ChirAuLC2**. Synchrotron radiation circular dichroism (SRCD) spectra of (g) **ChirAuLC1** recorded every 5 °C upon cooling from 100 °C to 30 °C, (h) mixture of 7.0 wt% **L2** in **L1** upon cooling from 100 °C to 60 °C.

deformed and the anisotropic LC groups orient preferentially perpendicular to the base of the lattice. In other words, XRD and TEM results show that the AuNPs self-assemble into ordered columnar structures. DSC investigations (see Fig. S8, ESI†) show for **ChirAuLC1** a wide and weak transition at 52.7 °C on heating, typical for such systems and associated with strongly reduced mobility of the LC groups.[26]

In OPM investigations, oily streaks appear in **ChirAuLC1** (see Fig. S9, ESI†) at room temperature, reminiscent of a cholesteric texture of the chiral nematic LC environment. **ChirAuLC1** exhibits birefringence after shearing. For **ChirAuLC2** only unspecific birefringence could be observed, attributed to the high viscosity of the NPs associated with the large gold content of the system. Based on these results having in view good miscibility with LC matrices, we focused on smaller nanoparticles for the detailed investigation of chirality. To establish whether there is a temperature effect, series of CD spectra were collected and are shown in Fig. 1g. The NPs synthesized with both chiral and LC groups show negative CD bands. The spectra of ligands on AuNPs show bands associated with the transitions of binaphthyl rings, the ^1B_b transition at 200 to 250 nm and the ^1L_b transition at 300 to 350 nm. In the CD spectra of **ChirAuLC1**, the **L2** ligands on AuNPs with (S)-configuration show intense negative Cotton effects for the ^1L_b transition.[36] The increase

of the CD signal intensity at 318 nm with lowering temperature is clearly evident, indicating the existence of helical twist in the mesophase of the columnar superstructure. The largest increase in ellipticity at 318 nm is detectable between 55 °C and 50 °C and this corresponds to the isotropic-mesophase transition temperature observed by DSC (see Fig. S8, ESI†). However, as the LC domains are very small and numerous, the contributions from linear dichroism and birefringence cancel out. This hypothesis is confirmed by rotating the sample in an interval of 90° (see in Fig. S10b, ESI†), only small changes of the CD signal occur at both 225 nm and 318 nm. This result excludes major contributions in the measurements of the possibly dominant effect of linear dichroism (birefringence), hence validating our approach.[26] The temperature-dependent intensity of the CD bands in **ChirAuLC1** weakens strongly at the first-order phase transition at 52.7 °C. The negative CD bands at 225 nm and 318 nm are not observed in solution (Fig. S11a, ESI†). The CD signals of **ChirAuLC1** in dichloromethane are positive, a sign opposite to that in a thin film. The difference between solution and thin film measurements and the temperature dependence of the thin film signals are indicative of helical twisting in the mesophase of **ChirAuLC1**. The positive CD signals of **ChirAuLC1** in dichloromethane are at similar wavelengths to the UV-Vis signals of **ChirAuLC1** in the same solution (Fig. S11b, ESI†). SRCD spectra of **ChirAuNP1** in thin films
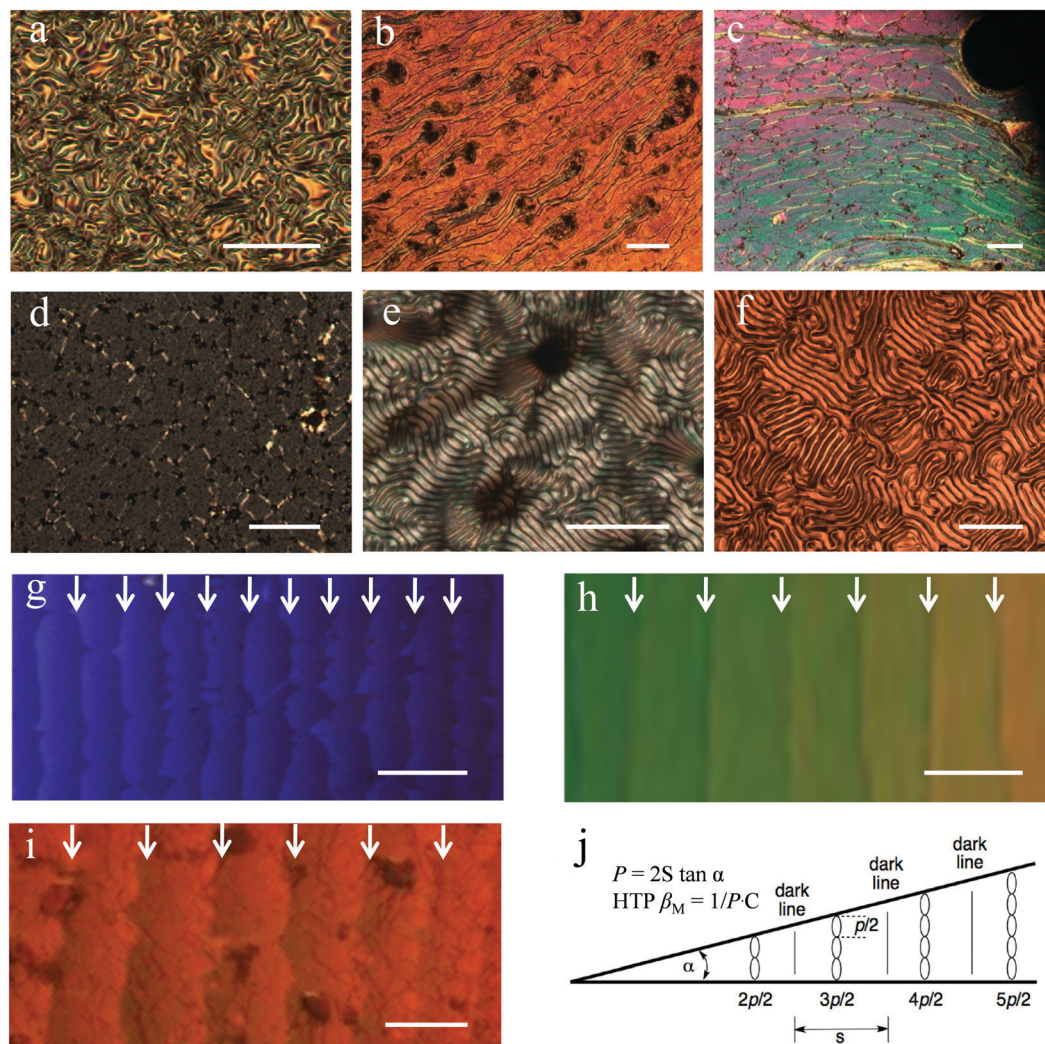
Fig. 2 Optical polarizing microscopy (OPM) micrographs of mesogen **L1** doped with (crossed polarizer) (a) 3.5 wt% **ChirAuLC1** (×50 μm) at 25 °C, (b) 6.5 wt% **ChirAuLC1** (×100 μm) at 25 °C, (c) 3.5 wt% **ChirAuNP1** (×100 μm) at 25 °C, (d) 6.5 wt% **ChirAuNP1** (×100 μm) at 25 °C. The induced N* phase in 5CB in a homeotropic cell (cell gap = 25 μm) doped with (e) 3.0 wt% of **ChirAuNP1** (×25 μm) at 30 °C, (f) 3.0 wt% of **ChirAuLC1** (×25 μm) at 30 °C. Images of Grandjean−Cano wedge cells showing Grandjean steps (lines) of the induced N* phase in mesogen **L1** doped with (g) 5.0 wt% free **L2** (×50 μm) at 25 °C, (h) 3.5 wt% **ChirAuNP1** (×50 μm) at 25 °C, (i) 6.5 wt% **ChirAuLC1** (×50 μm) at 25 °C, (j) Grandjean−Cano wedge cell method to determine the helical pitch (P) of the N* phase (S = distance between two disclination lines), and the calculation of the helical twisting power HTP (β_M, a measure for the ability of a chiral dopant to twist a nematic LC phase) followed by the helical pitch measurements, where C is the molar concentration of the chiral additive.

(see in Fig. S10a, ESI†) shows weak CD signals unaffected by temperature. To test our hypothesis of helical twisting in the LC state **ChirAuLC1** further a composition consisting of 7.0 wt% **L2** in **L1** was measured. This showed upon cooling from 80 °C to 60 °C (Fig. 2h), that the characteristic negative CD signals are located at 240 and 336 nm and the CD intensity is independent of temperature. We note that the CD intensity of **ChirAuLC1** could be linked to the interactions of ligands with the surface of AuNPs as discussed earlier.[27,37] The metal and ligand-to-metal charge transfer transitions induce the blue shifted CD band at 318 nm for **ChirAuLC1** compared to the 335 nm for the mixture of 7.0 wt% **L2** in **L1** (Fig. 2g and h). On further cooling, the mixture of 7.0 wt% **L2** in **L1** transitioned to the chiral nematic (N*) phase. The CD intensity (see Fig. S12, ESI†) was enhanced by almost three orders of magnitude on this transition,

(see OPM picture in Fig. S2d showing high birefringence, ESI†). The CD bands in chiral nematics outside the chromophoric absorption region have been associated with scattering effects.[38] The strong CD signal is close to 400 nm at 40 °C and this is of a similar value as the reflective band related to the pitch p of the cholesteric helix by the relation, $\lambda = np$, where n is the average refractive index of the mesophase.

To investigate **ChirAuLC1** in more detail thermo-gravimetric analysis (TGA) was performed, giving (Fig. S13a, ESI†) the weight fraction of gold in **ChirAuLC1** as 60.6 wt%. Ligand and mesogen density per Au NP were calculated (see ESI,† part 3) based on the combination of ^{1}H-NMR analysis (see Fig. S7, ESI†) and the model developed by Gelbart *et al.*[39] The average diameter of the gold cores for **AuNP1** is 1.9 nm (see Fig. S3, ESI†). Based on this data we calculated that there are on average

211 Au atoms per particle, and a total number of 53 ligands per particle, of which 9 are **L2**, 22 are 1-hexanethiol groups and 22 are **L1** for **ChirAuLC1**. This is in accord with a ligand density of up to 6.3 ligands per nm² on the NP surface.[40] A similar calculation was performed for **ChirAuNP1** and there are 28 **L2** groups and 25 1-hexanethiol chains per NP. These results allow us to determine the average number of organic ligands present in a given NP–LC system. This in turn permits us to measure the effectiveness of inducing the N* phase by **ChirAuNP**, **ChirAuLC** and free **L2** into a nematic matrix. For comparison the doping effects of **L2** in **L1** were studied too (see Fig. S2, ESI†). An obvious chiral nematic phase (N*) is evidenced by bundles of unique oily streaks with a wide range of **L2** mass ratio in **L1** up to 7.0% (wt/wt%).

In Fig. 2a–d, OPM textures of **ChirAuNP1** and **ChirAuLC1** mixed with **L1** between untreated glass slides provide the first insight in the chiral properties of the NP–LC systems. All NPs disperse well in the LC host without obvious aggregation or segregation. For 1.0 wt% of **ChirAuLC1** in **L1**, a Schlieren texture was observed (see in Fig. S15a, ESI†), attributed to a helical pitch in length beyond the visible range. When the concentration of **ChirAuLC1** in **L1** is increased to 3.5 wt%, a fingerprint-like texture occurs corresponding to the N* phase (Fig. 2a). For 6.5 wt% of **ChirAuLC1** in **L1** (Fig. 2b), the texture was observed to selectively reflect light indicative of a helical pitch at the visible light length scales. In Fig. 2c, distinct oily streaks indicate that the N* phase appeared at concentrations as low as 3.5 wt% of **ChirAuNP1**. However, for 6.5 wt% of **ChirAuNP1** in **L1** (Fig. 2d), the characteristic cholesteric colour was absent with the pitch being shorter than visible wavelengths. Generally, both **ChirAuNPs** and **ChirAuLC** can be employed as chiral dopants or chiral additives to induce the N* phase in achiral LC hosts.[41]

Using the Cano wedge cell technique for pitch determination, where a wedge cell with known angle and uniform disclination lines is required,[41] allowed us to quantify the efficiency of chiral transfer from the NPs to the host **L1** (see Fig. 2g–j).[42] The helical pitch values for the N* phase induced by **L2**, **ChirAuNP1** and **ChirAuLC1** depend on their concentration in the LC host. Based on the OPM observations, shown in Fig. 2a–d and Fig. S2 (ESI†), different mass ratios of chiral dopants (5.0 wt% **L2**, 3.5 wt% **ChirAuNP1** and 6.5 wt% **ChirAuLC1**) were chosen to prepare wedge-cells. The distance between adjacent lines in Fig. 2g–i is 24.1 μm, 37.7 μm and 47.5 μm, respectively. The HTP values of **L2**, **ChirAuNP1** and **ChirAuLC1** were calculated by the classical equation ($P = 2S \tan \alpha$, where P = pitch, S = distance between two disclination lines, α = opening angle of the cell). The obtained HTP values (see Table 1) are 32.1 μm⁻¹ for **L2**, 3910.0 μm⁻¹ for **ChirAuNP1** and 1668.7 μm⁻¹ for **ChirAuLC1**, respectively. As the calculation of the HTP is based on molar fractions, significantly larger values are obtained for both **ChirAuNP1** and **ChirAuLC1** than for free **L2**. Here, we show that a combination of highly chiral ligands together with suitable LC ligands enhances the macrochirality of comparable chiral NPs significantly further. The synergistic interaction of chiral centres with LC groups on NPs exerts a twisted but flexible ligand shell closely adjusted to molecular parameters of the LC matrix.

Table 1 Helical twisting power (HTP β_M) values (μm⁻¹) of **L2**, **ChirAuLC1** and **ChirAuNP1** in host mesogen **L1**

Type	HTP β_M/μm⁻¹	HTP $\beta_{M/L2}$[b]/μm⁻¹ chiral ligand⁻¹	HTP β_W[c]/μm⁻¹	HTP $\beta_{W/L2}$[d]/μm⁻¹
DS1[a]	19.7	19.7	4.9	4.9
NP1 (45 DS1)[a]	1522.1	34.0	3.2	7.8
L2	32.1	32.1	50.0	50.0
ChirAuLC1 (9 **L2**)	1668.7	185.4	19.5	320.7
ChirAuNP1 (28 **L2**)	3910.0	139.6	49.6	234.2

[a] Normalized values are from the ref. 43. [b] HTP $\beta_{M/L2}$/μm⁻¹ chiral ligand⁻¹ is the normalized HTP value for per chiral group (**L2**). [c] HTP β_W/μm⁻¹ is the normalized HTP value for the chiral NPs in host mesogen **L1** based on weight concentration. [d] HTP $\beta_{W/L2}$/μm⁻¹ is the normalized HTP value for the chiral group (**L2**) in host mesogen **L1** based on weight concentration. HTP β_M is obtained based on molar concentration while HTP β_W is evaluated based on weight concentration.

Such already helically oriented chiral patterns facilitate the helical distortion through interactions with the surrounding LC host molecules and maintain the helical twist throughout this elastic medium over large distances. This enables suitably functionalized NPs to induce the N* phase with high efficiency and this can be viewed rationally as macro-chiral.[27] Based on the experiments the number of **L2** on **ChirAuNP1** (28 per particle) is 3.1 times higher than that in **ChirAuLC1** (9 per particle). In Table 1, the HTP values of the systems measured here together with those reported by Hegmann et al.,[43] as comparable NPs are listed. The significant difference between low molar mass ligands such as **L2** (or DS1 in ref. 43) and chiral ligands attached to NPs is that for NP systems much higher values for the HTP are reached. For **ChirAuLC1** a value of 1668.7 (β_M/μm⁻¹) and for **ChirAuNP1** a value of 3910.0 (β_M/μm⁻¹) is obtained; broadly similar to what was reported by Hegmann et al.[43] for different ligands. This increased chirality amplification could be described by the effects of a distributed chiral surface on the functionalized NPs. This is the certain case for NPs not functionalized with LC groups. When the normalized HTP values ($\beta_{M/L2}$/μm⁻¹ chiral ligand⁻¹ and $\beta_{W/L2}$/μm⁻¹) were used to measure the helical twisting power of **L2** group attached to the NPs, as in our case, a second effect is measurable. When compared to free **L2**, the HTP value of **ChirAuNP1** is amplified by ∼×4.3 times and an even higher value of ∼×5.8 times for **ChirAuLC1** ([b]HTP $\beta_{M/L2}$/μm⁻¹ chiral ligand⁻¹) is found. When the HTP values were calculated by weight concentration ($\beta_{W/L2}$/μm⁻¹), **ChirAuLC1** shows a value of ∼×6.4 times higher than the HTP of free **L2** and that of **ChirAuNP1** is ∼×4.7 times larger than that of **L2**. Both evaluation methods show that **ChirAuLC1** transfers chirality more effectively than **ChirAuNP1** to the host nematogen **L1**. We attribute this further amplification to the contributing factor of the LC groups. The LC groups (**L1**) on AuNPs enhance their miscibility in the matrix **L1** and this results in the enhanced chiral signal transfer. The LC groups **L1** attached to the NPs are chirally perturbed by **L2** and effectively a synergistic combination of a distributed surface effect with the domino/sergeant-soldier effect occurs in the anisotropic matrix.

To test the general applicability of the system the widely utilized nematic liquid crystal 5CB (see Chart 1), was chosen as

Table 2 Helical twisting power (HTP β_M) values (μm^{-1}) of **ChirAuNP1** and **ChirAuLC1** in host mesogen 5CB

Type	HTP $\beta_M{}^a$/ μm^{-1}	HTP $\beta_{M/L2}{}^b$/μm^{-1} chiral ligand^{-1}	HTP $\beta_W{}^c$/ μm^{-1}	HTP $\beta_{W/L2}{}^d$/ μm^{-1}
ChirAuLC1 (9 **L2**)	1064.5	118.3	4.3	71.2
ChirAuNP1 (28 **L2**)	1788.1	63.6	8.1	38.4

^{a} HTP β_M/μm^{-1} is the normalized HTP value for the chiral NPs in host mesogen 5CB. ^{b} HTP $\beta_{M/L2}$/μm^{-1} chiral ligand^{-1} is the normalized HTP value for per chiral group (**L2**). ^{c} HTP β_W/μm^{-1} is the normalized HTP value for the chiral NPs in host mesogen 5CB based on weight concentration. ^{d} HTP $\beta_{W/L2}$/μm^{-1} is the normalized HTP value for chiral groups in host 5CB system based on weight concentration. HTP β_M is obtained based on molar concentration while HTP β_W is evaluated based on weight concentration.

the second test host to validate if the functionalized NPs could amplify chirality effectively beyond the optimized system **L1**.[44] As shown in Fig. 2e and f, both **ChirAuNP1** and **ChirAuLC1** induce well-defined fingerprint textures permitting helical pitch measurements.[41] The helical pitch of 5CB doped with 3.0 wt% **ChirAuNP1** and a composition doped with 3.0 wt% **ChirAuLC1** was measured as 4.1 μm and 7.7 μm, respectively. The HTP values of **ChirAuNP1** and **ChirAuLC1** can thus be calculated to be 1788.1 μm^{-1} and 1064.5 μm^{-1}, respectively, using the methods described above. The HTP values of **ChirAuNP1** and **ChirAuLC1** in the host 5CB are lower than that in the mesogen system **L1**. Both normalized HTP values ($\beta_{M/L2}$/μm^{-1} chiral ligand^{-1} and $\beta_{W/L2}$/μm^{-1}) of **L2** groups for **ChirAuLC1** are almost 2 times higher than that for **ChirAuNP1** (Table 2). We note that the NPs in 5CB host, especially **ChirAuNP1**, do not orient as well as in **L1** host, attributed to somewhat higher tendency of the NPs to segregate. This highlights the importance of the optimal selection of the NP surface matching the liquid crystal matrix. We note too that the measured values for **ChirAuLC1** reported here are considerably larger (higher by a factor of ~26.5–38.2 depending on the system) than those we reported for structurally related LC oligomers in the host 5CB where HTP values of 27.9–40.2 were determined.[45] This confirms the synergistic effect of NPs functionalized with chiral groups and LC ligands for chirality transfer. This modular approach where chiral groups attached to NP surfaces transfer chiral organisation to LC ligands bound too to the NPs enhances the overall chirality transfer to non chiral matrices. This modified "sergeant-soldier" approach amplifies the macro-chirality of the NP surfaces by LC groups interacting with enhanced efficiency with matrices.

To conclude, we have demonstrated that it is possible to obtain macro-chiral AuNPs by modifying NPs with both LC groups and chiral groups. Facilitated by attached LC groups, NPs self-assemble into columnar arrangements and helical twist superstructures are formed by these NPs, evidenced by SRCD spectroscopy. When doped in nematic LC hosts, NPs transfer the chirality into the surrounding medium with high efficiency and show enhanced macro-chiral properties. Furthermore, the devised NP–LC system serves as a platform to visualize and measure the chirality transfer of NPs. We believe this simple and potentially universal design strategy on NPs provides a new way to fabricate functional materials with potential applications in metamaterials, catalysts and smart sensors.

Conflicts of interest

There are no conflicts to declare.

Acknowledgements

Notes and references

1 M. Kato and S. L. McKnight, *Annu. Rev. Biochem.*, 2018, **87**, 351–390.
2 A. Hu, J. Guo, H. Pan, H. Tang, Z. Gao and Z. Zuo, *J. Am. Chem. Soc.*, 2018, **140**, 1612–1616.
3 T. G. W. Edwardson, K. L. Lau, D. Bousmail, C. J. Serpell and H. F. Sleiman, *Nat. Chem.*, 2016, **8**, 162.
4 F. Crick, *Nature*, 1970, **227**, 561–563.
5 J. I. Kwiecińska and M. Cieplak, *J. Phys.: Condens. Matter*, 2005, **17**, 1565–1580.
6 J. Adamcik and R. Mezzenga, *Angew. Chem., Int. Ed.*, 2018, **57**, 8370–8382.
7 S. Damodaran and K. L. Parki, *Fennema's Food Chemistry*, 2017, pp. 235–356.
8 P. S. Huang, S. E. Boyken and D. Baker, *Nature*, 2016, **537**, 320.
9 Y. H. Chen, Y. J. Chen and C. Y. Hsieh, *US Pat.*, US9348179B2, 2016.
10 J. Li, H. K. Bisoyi, J. Tian, J. Guo and Q. Li, *Adv. Mater.*, 2019, **31**, 1807751.
11 S. Tokunaga, Y. Itoh, H. Tanaka, F. Araoka and T. Aida, *J. Am. Chem. Soc.*, 2018, **140**, 10946–10949.
12 J. Li, Z. Zhang, J. Tian, G. Li, J. Wei and J. Guo, *Adv. Opt. Mater.*, 2017, **5**, 1700014.
13 S. Tokunaga, Y. Itoh, Y. Yaguchi, H. Tanaka, F. Araoka, H. Takezoe and T. Aida, *Adv. Mater.*, 2016, **28**, 4077–4083.
14 A. Chandran, J. Prakash, J. Gangwar, T. Joshi, A. K. Srivastava, D. Haranath and A. M. Biradar, *RSC Adv.*, 2016, **6**, 53873–53881.
15 H. Qi and T. Hegmann, *J. Mater. Chem.*, 2006, **16**, 4197–4205.
16 Ł. Duda, M. Czajkowski, B. Potaniec and P. Vaňkátová, *Liq. Cryst.*, 2019, 1–11.
17 K. J. Koch, F. C. Gozzo, S. C. Nanita, Z. Takats, M. N. Eberlin and R. G. Cooks, *Angew. Chem., Int. Ed.*, 2002, **41**, 1721–1724.
18 K. Tamura and P. R. Schimmel, *Proc. Natl. Acad. Sci. U. S. A.*, 2006, **103**, 13750–13752.
19 N. Hosono, A. R. A. Palmans and E. W. Meijer, *Chem. Commun.*, 2014, **50**, 7990–7993.
20 K. Tahara, A. Noguchi, R. Nakayama, E. Ghijsens, S. D. Feyter and Y. Tobe, *Angew. Chem., Int. Ed.*, 2019, **58**, 7733–7738.
21 A. Minoia, I. Destoop, E. Ghijsens, S. D. Feyter, K. Tahara, Y. Tobe and R. Lazzaroni, *RSC Adv.*, 2015, **5**, 6642–6646.

22 A. Choudhary, G. Singh and A. M. Biradar, *Nanoscale*, 2014, **6**, 7743–7756.

23 P. V. D. Witte, J. C. Galan and J. Lub, *Liq. Cryst.*, 1998, **24**, 819–827.

24 J. Yan, F. Ota, B. A. S. Jose and K. Akagi, *Adv. Funct. Mater.*, 2017, **27**, 1604529.

25 J. Yoshida, S. Tamura, H. Yuge and G. Watanabe, *Soft Matter*, 2018, **14**, 27–30.

26 L. Cseh, X. Mang, X. Zeng, F. Liu, G. H. Mehl, G. Ungar and G. Siligardi, *J. Am. Chem. Soc.*, 2015, **137**, 12736–12739.

27 A. Nemati, S. Shadpour, L. Querciagrossa, L. Li, T. Mori, M. Gao, C. Zannoni and T. Hegmann, *Nat. Commun.*, 2018, **9**, 3908.

28 S. Mischler, S. Guerra and R. Deschenaux, *Chem. Commun.*, 2012, **48**, 2183–2185.

29 R. Eelkema and B. L. Feringa, *Org. Biomol. Chem.*, 2006, **4**, 3729–3745.

30 Y. Kim, M. Frigoli, N. Vanthuyne and N. Tamaoki, *Chem. Commun.*, 2017, **53**, 200–203.

31 T. Kosa, V. H. Bodnar, B. Taheri and P. Palffy-Muhoray, *Mol. Cryst. Liq. Cryst.*, 2001, **369**, 129–137.

32 D. Podolskyy, O. Banji and P. Rudquist, *Liq. Cryst.*, 2008, **35**, 789–791.

33 L. Cseh and G. H. Mehl, *J. Am. Chem. Soc.*, 2006, **128**, 13376–13377.

34 S. Link and M. El-Sayed, *J. Phys. Chem. B*, 1999, **103**, 4212–4217.

35 S. Kango, S. Kalia, A. Celli, J. Njuguna, Y. Habibi and R. Kumar, *Prog. Polym. Sci.*, 2013, **38**, 1232–1261.

36 T. Yamada, M. Ohshima, K. Yuasa, T. Kikuchi and R. Tanaka, *Mar. Drugs*, 2016, **14**, 74.

37 I. Russier-Antoine, F. Bertorelle, A. Kulesza, A. Soleilhac, A. Bensalah-Ledoux, S. Guy, P. Dugourd, P. Brevet and R. Antoine, *Prog. Nat. Sci: Mater.*, 2016, **26**, 455–460.

38 G. Gottarelli, S. Lena, S. Masiero, S. Pieraccini and G. P. Spada, *Chirality*, 2008, **20**, 471–485.

39 D. V. Leff, P. C. Ohara, J. R. Heath and W. M. Gelbart, *J. Phys. Chem.*, 1995, **99**, 7036–7041.

40 M. J. Hostetler, S. J. Green, J. J. Stokes and R. Murray, *J. Am. Chem. Soc.*, 1996, **118**, 4212–4213.

41 C. Kühn, M. Bremer and P. R. Schreiner, *Liq. Cryst.*, 2019, **46**, 1763–1768.

42 I. Dierking, *Textures of Liquid Crystals*, John Wiley & Sons, 2003.

43 A. Sharma, T. Mori, H. C. Lee, M. Worden, E. Bidwell and T. Hegmann, *ACS Nano*, 2014, **8**, 11966–11976.

44 A. Mouhli, H. Ayeb, T. Othman, J. Fresnais, V. Dupuis, I. Nemitz, J. Pendery, C. Rosenblatt, O. Sandre and E. Lacaze, *Phys. Rev. E.*, 2017, **96**, 012706.

45 C. J. Schubert, M. G. Tamba and G. H. Mehl, *Chem. Commun.*, 2012, **48**, 6851–6853.